Astron. Astrophys. 346, 892–896 (1999)

ASTRONOMY AND ASTROPHYSICS

Spatially resolved spectroscopy of Z Canis Majoris components⋆

P.J.V. Garcia[1,2], **E. Thiébaut**[1], **and R. Bacon**[1]

[1] CRAL/Observatoire de Lyon, CNRS UMR 5574, 9 avenue Charles André, F-69561 St. Genis-Laval Cedex, France
[2] Centro de Astrofísica da Universidade do Porto, Rua das Estrelas S/N, 4150 Porto, Portugal

Received 14 January 1999 / Accepted 21 April 1999

Abstract. We present adaptive optics integral field spectrograph observations of the Z CMa binary in the 6203 Å-6528 Å band with a spectral resolution of 3200 and spatial resolution of 0.24″, made with the OASIS instrument coupled to the PUE'O bonnette.

Using the binary parameters derived from speckle interferometry, we are able to recover the spectrum of each component, in spite of a spatial sampling (0.11″) similar to the system separation (0.1″). The component that dominates the optical continuum presents a spectrum similar to the one from the system in its pre-outburst phase. The other component (so-called "IR companion") shows an emission line spectrum. Extended emission is detected in [OI]λ6300. This emission presents an unresolved peak plus an elongated structure, similar to that found in Classical T Tauri Stars' microjets. The low velocity component is unresolved and slightly shifted from the stellar continuum location. The high velocity component is extended but also contributes to the unresolved peak. This microjet is spatially associated with the infrared companion and with the system's powerful parsec-scale jet. The upper limit of the microjet width is 0.24″, and its length is $\sim 1''$. This size combined with the material velocity results in a dynamical time scale of ~ 10 yrs, compatible with its origin in the 1987 outburst.

Key words: stars: individual: Z CMa – stars: formation – ISM: jets and outflows – stars: pre-main sequence – techniques: spectroscopic

1. Introduction

Z CMa is a pre-main-sequence (Herbig, 1960) binary (Koresko et al., 1991) located at a distance of 1150 pc (Clariá 1974). One component, *the secondary*, dominates the continuum at optical wavelengths (Thiébaut, 1994, Barth et al., 1994, Thiébaut et al., 1995) whereas *the primary* dominates the IR continuum and total luminosity of the system (Koresko et al., 1991). The secondary is an FU Ori object (Hartmann et al., 1989), and the primary is a Herbig Ae/Be star (Withney et al., 1993, hereinafter refered as W93).

The system is associated with a powerful bipolar jet that extends up to 2 pc along position angle 60 deg (Poetzel et al., 1989). In 1987 Z CMa suffered an outburst in which the typical FU Ori absorption line spectrum changed into an emission line spectrum on top of a bluer continuum (Hessmann et al., 1991). Spectropolarimetry observations showed that the emission lines were more polarized than the continuum (W93). This was interpreted as an evidence for their origin in the embedded companion. This interpretation also had the advantage of attributing the outburst to the primary thus solving several difficulties in explaining the emission line spectra in the FU Ori scenario (Hessmann et al.). However, Fischer et al. (1998) found that at 2.2 μm both components are polarized, the secondary having the *higher* intrinsic polarization. In order to explain both their observations and W93's assumption that the secondary has a negligible contribution to the optical polarization, they invoked an inclined and flared thick disk for the secondary. Recently Lamzin et al. (1998) argued that the emission lines originate from the secondary and that the higher polarization results from Thompson scattering in the wind, thus opening the discussion of which component is the emission line object.

Here we present integral field spectrographic observations of the Z CMa system using OASIS[1], coupled to the PUE'O adaptive optics bonnette (Rigaut et al., 1998). These observations allowed us to image the jet with a 0.24″ resolution, and to measure the image centroids with an accuracy beyond the telescope diffraction limit (which is 0.036″ for the CFHT at [OI]). We combined this information with the binary parameters derived from speckle interferometry to recover for the first time the spectrum of each Z CMa component.

2. Observations and data reduction

We observed ZCMa at the CFHT, on January 23rd 1998 during a commissioning night of the integral field spectrograph OASIS coupled to the adaptive optics bonette PUE'O.

In the TIGER mode (Bacon et al., 1995) of the OASIS instrument the field of view is sampled by an array of micro-lenses. The image produced by each micro-lens is then dispersed with

Send offprint requests to: pgarcia@obs.univ-lyon1.fr

⋆ Based on observations collected at the Canada-France-Hawaii Telescope, operated by the National Research Council of Canada, the Centre National de la Recherche Scientifique, and University of Hawaii.

[1] Manual and instrument description available on-line at: `http://www-obs.univ-lyon1.fr/~oasis/home/`

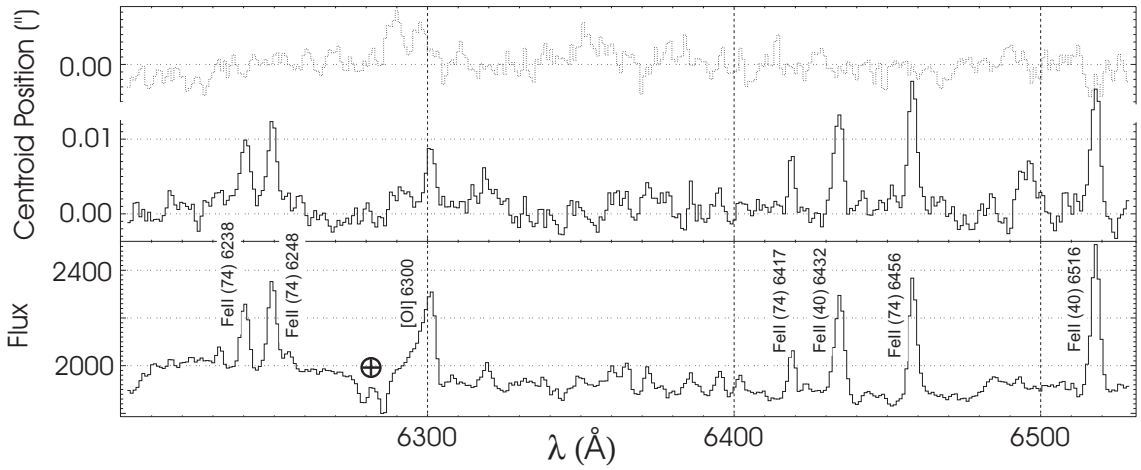

Fig. 1. The bottom graph is the integrated Z CMa system spectrum $F_{\rm total}$ (flux in arbitrary units). In the upper and middle graph we plot the centroid position, in the system reference frame, units are in arc sec. The upper graph (dotted) is the centroid in the axis perpendicular to the line joining the components (positive direction pointing to the jet). The middle graph (solid) is the centroid along the binary axis (positive direction pointing to the primary).

a grism and filtered with a large bandpass filter to avoid the overlapping of spectra on the CCD. An OASIS configuration is defined by the sky projected micro-lens separation, the filter, and grism used. Each configuration must be calibrated with additional frames taken at zenith: undispersed micro-pupils, halogen lamp and associated arc, flux standard and associated arc. Because the configuration calibrations are, in general, done at different zenithal angles from the science target, each science exposure must be preceded/followed by an arc exposure to correct for instrument flexure effects in the wavelength solution.

The OASIS configuration used covered the 6200-6532 Å range with a spectral resolution of 3200; the sky sampling was 0.11″/microlens and the field of view $4.1'' \times 3.3''$. We took a 300 s exposure of Z CMa followed, at the same telescope position, by a neon arc calibration frame. These exposures were complemented by the standard configuration calibration frames.

The data were processed according to the standard OASIS procedures within the XOasis software. The raw CCD images were offset and bias subtracted. The micro-lenses' positions on the CCD were computed using the micro-pupil frame taken without the grism and filter wheel, the optics distortion corrected, then the spectra crests were found in the halogen frame. Using the previous information and the arc frame associated with the halogen exposure, a model for the spectrograph optics was fitted and the extraction mask created.

The 1100 Z CMa spectra were then extracted from the CCD frame and wavelength calibrated, using the mask and Z CMa associated neon arc, thus creating a raw TIGER data cube. Cosmic rays were removed from the raw cube. These procedures were repeated for the halogen and photometric standard, which were needed to calibrate the Z CMa raw cube for the spatial and spectral dependence of the instrument transmission.

3. Results and discussion

3.1. Integrated spectra

In Fig. 1 we present the Z CMa integrated spectra, i.e., the projection of the data cube on the wavelength axis. The [OI]λ6300 Å line is visible, with its high velocity wing contaminated by telluric absorption. However, the telluric [OI] emission contribution to the line is negligible. Several FeII lines are also present (Hessmann et al., 1991).

3.2. Cube Gauss fitting and component spectrum recovery

We fitted each monochromatic image with a 2D circular gaussian. This allowed us to estimate a 0.63″ FWHM spatial resolution by assuming that these images were unresolved. The precision in the gaussian centroid position was 0.002″.

The evolution of the gaussian centroid with wavelength when compared to the spectra revealed that the continuum shifts in the direction of the atmospheric differential refraction – ADR (eg. Filippenko, 1982). The emission lines however have a different behavior: they shift proportionally to their intensity in the direction of the primary. We thus fitted the continuum centroids versus wavelength with a *straight line* and applied the correction to the cube thus removing the *linear* ADR drift (the paragalactic angle varied only $\sim 1.3^\circ$ during the exposure and could be negleted). In Fig. 1 we plot the ADR corrected gaussian centroid position versus wavelength in the binary system frame. All the emission lines except [OI] are associated with shifts in the primary direction without any counterpart in the perpendicular direction. This is due to a lever effect from the primary emission in the fit. The primary is responsible for the emission line component in the integrated spectra and the secondary dominates in the continuum. This is in agreement with the speckle observations, the spectropolarimetric data interpre-

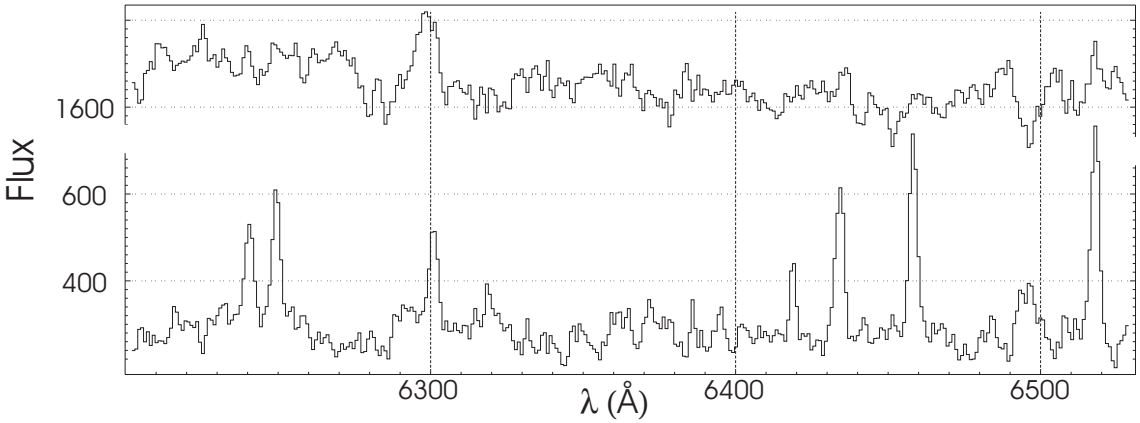

Fig. 2. Recovered spectrum for each system component. The upper spectrum is from the secondary – the FU Ori object, it presents several similarities with the pre-outburst system spectrum. The lower spectrum is from the primary – the Herbig Ae/Be star, strong emission lines are present.

tation and recent observations by Bailey (1998), who measured centroid shifts, from long slit spectroscopy, of Z CMa.

Appendix A demonstrates that the fitted gaussian centroids measure the system barycenter. Hence, our centroid and system spectrum measurements can be combined with the information derived from the speckle data to recover the spectra of each component. Our raw centroid measurements are by definition:

$$C_{\rm raw}(\lambda) = \frac{F_1(\lambda)\,x_1 + F_2(\lambda)\,x_2}{F_{\rm total}(\lambda)} = x_1 + \frac{F_2(\lambda)}{F_{\rm total}(\lambda)}\,\rho \qquad (1)$$

where $F_1(\lambda)$ and $F_2(\lambda)$ are the monochromatic fluxes of the primary and secondary, $F_{\rm total}(\lambda) = F_1(\lambda) + F_2(\lambda)$ the system flux, x_1 and x_2 the primary and secondary positions and $\rho = x_2 - x_1$ the system separation. In the *continuum* and for our small wavelength range (∼300 Å) the previous expression does not depend on λ:

$$C^{\rm cont}_{\rm raw} = \frac{F^{\rm cont}_1\,x_1 + F^{\rm cont}_2\,x_2}{F^{\rm cont}_{\rm total}} = x_1 + \frac{r}{1+r}\,\rho \qquad (2)$$

where $r = F^{\rm cont}_2/F^{\rm cont}_1$ is the flux ratio of the components in the continuum. The previous expressions can be combined with the information derived from the speckle data (r and ρ) to recover the spectrum of each component:

$$F_1(\lambda) = (1/(1+r) + C(\lambda)/\rho)F_{\rm total}(\lambda) \qquad (3)$$

$$F_2(\lambda) = (r/(1+r) - C(\lambda)/\rho)F_{\rm total}(\lambda) \qquad (4)$$

where $C(\lambda) = C_{\rm raw}(\lambda) - C^{\rm cont}_{\rm raw}$, is the centroid shift, in the system axis, relative to the continuum centroid position (which is computed by taking the median of all points with a shift smaller than the average). If the flux ratio at a given wavelength r_λ equals the continuum ratio r we recover $C = 0$. However, the trick of the method is that, because each object has a diferent spectra, locally we have $r_\lambda \neq r$ (due to the emission/absorption lines). As a consequence, $C(\lambda)$ changes with wavelength as observed in (Fig. 1). Our measurements yield C and $F_{\rm total}$ (see Fig. 1), using the speckle data in the same wavelength we get $r = 7.2 \pm 1.3$ and $\rho = 0.102'' \pm 0.004''$ (Thiébaut, 1994, Barth et al., 1994, Thiébaut et al., 1995).

In Fig. 2 we plot the recovered spectrum of both components. The typical (median) error for the primary reconstructed spectrum is 18% (decreasing to 12% in the emission lines). The variance is dominated (∼65%) by the magnitude ratio error which we took as 0.2 mag. The secondary spectrum reconstruction error is 3%.

The primary is the emission line object. The spectrum of the secondary presents several absorption features that were visible in the low state system spectrum. The broad absorption complex seen at ~ 6495 Å was present in the low state spectrum – Fig. 2 of Hartmann et al., 1989 and no sign of it is present in the system integrated spectrum presented in our Fig. 1. The absorption features seen at ~ 6440 Å and at ~ 6451 Å and already hinted in the integrated spectrum were also present in Welty et al., 1992 low state spectrum (their Fig. 3).

3.3. The [OI]λ6300 jet

The [OI] emission in the reconstructed spectra shows a more complex behavior. In Fig. 1, the centroid shifts at the [OI] position move *away* from the secondary *towards* the primary. This shows that the primary drives the jet. Furthermore there is also a significant shift in the direction perpendicular to the system axis. This shift is in agreement with Bailey (1998), who found that in his long slit centroid measurements the [NII] and [SII] emission lines profiles are dominated by the jet. These [OI] shifts in the perpendicular direction imply that the reconstructed spectra in the [OI] region are not correct because we assume that all the emission is concentrated in the binary. Furthermore they hint a more complex structure for the [OI] emission region.

We integrated spectrally the [OI] line in the (-570 km s^{-1} $\leq v \leq$ 160 km s^{-1}) interval and subtracted the resultant image with a PSF obtained by integrating the line-free range of the spectra (6260 Å– 6270 Å). The resulting image, already slightly elongated in the jet direction, was deconvolved using the `lucy`

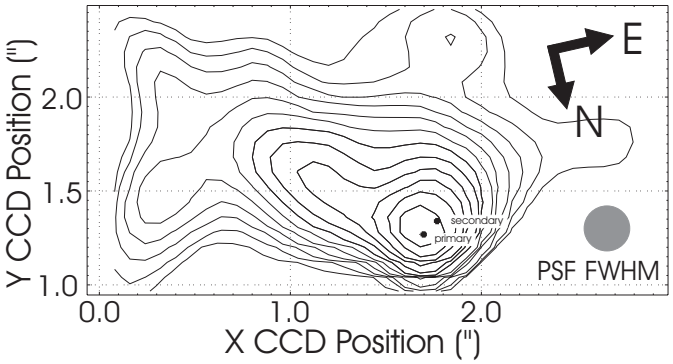

Fig. 3. Deconvolved [OI] emission image. The first contour starts at max/2.5, the other contours are decreasing by factors of 2.5. The axis of the jet passes trough the primary.

procedure (Snyder et al., 1993) in IRAF/STDAS[2]. `lucy` requires a noise estimation and a background subtracted image. The histogram of the image to deconvolve was fitted with a gaussian, thus measuring the sigma and centroid. These were used, respectively, as noise and background estimators. The final resolution (FWHM) for the deconvolved image was 0.24″, convergence being obtained after 26 iterations.

Fig. 3 shows the deconvolved image, the jet is clearly visible, it points in the expected direction: position angle $\sim 240^\circ$ and extends to the limit of our field of view were it gets contaminated by a deconvolution edge artifact (the broadening at $0'' \leq X_{\rm ccd} \leq 0.5''$). The jet axis points to the embedded primary and originates from an unresolved peak coincident with the system. We deconvolved the integrated cube in the [OI] line (-570 km s^{-1} $\leq v \leq$ -120 km s^{-1}) zone and this peak is still present. The integrated cube at lower velocities (-120 km s^{-1} $\leq v \leq$ 160 km s^{-1}) was deconvolved and found unresolved. The origin of this peak can be twofold: due to a continuum underestimation in the subtraction or because the jet is already "super-alfvénic" at our spatial resolution of 230 AU. Our precision in the continuum subtraction precludes the first possibility. The second is supported both from jet theory, where the jet is already super-alfvénic at linear scales of the order of 10 AU (e.g., Ferreira 1997), whose synthetic [OI] jet maps (Cabrit et al., 1999) have a morphology very similar to our observations and, from integral field spectroscopy observations of DG Tau (Lavalley et al., 1997) and long slit spectroscopy of CTTSs (Hirth et al., 1997). It should be pointed that our precision for the *center* of this peak is $\sim$0.1″, although our precision in the subtraction is enough to validate the existence of the unresolved peak. This low precision originates from the continuum subtraction – variations of 2% in the continuum will cause shifts of 0.03″ in the unresolved component position (the jet however is *unaffected*).

We fitted the jet width along the jet axis with a gaussian and found it to be unresolved. Typical jet widths for Taurus CTTSs at similar distances from the central source are ≤ 40 AU (Ray et al., 1996) which would be unresolved at the Z CMa distance.

It is worth notice that the microjet probed by our observations $\sim$ 1″ has a dynamical time scale (assuming $v \sim$500 km s^{-1} from the [OI] line profile) of ~ 10 yr. We associate this material to the 1987 outburst ejecta.

4. Conclusions

We observed Z CMa with the integral field spectrograph OASIS coupled to the adaptive optics bonette PUE'O.

The image centroid evolution with wavelength was measured with a super resolution of $0.002''$. Using the binary parameters derived from speckle interferometry observations at similar wavelengths we were able to recover the spectra of each component. The primary emerges as the emission line object and the secondary (optical primary) presents a spectrum typical of the system before the 1987 outburst.

Z CMa jet was imaged at a 0.24″ resolution in the [OI]λ6300. It consists of an elongated structure whose width is unresolved and whose axis passes through the primary, and of an unresolved base with a wide range in velocities. This morphology is similar to Classical TTauri Stars' microjets. The part of the jet sampled by our observations is associated with the material ejected in the 1987 outburst.

We have shown that, for pre-main sequence binaries whose system parameters (separation and flux ratio) are known from broad band high angular resolution observations, integral field spectroscopy can recover their spectra for separations up to 6 times smaller than the actual IFS+AO angular resolution. This technique is very promising for the study of activity in close pre-main sequence binaries.

Acknowledgements. PJVG acknowledges support from the Portuguese Fundação para a Ciência e Tecnologia through grant PRAXIS XXI/BD/5780/95. The authors thank Renaud Foy and Andreii Tokovinine for a critical reading of the manuscript, the referee for useful comments that clarified the text, the TIGER Team for support during the data reduction process and D. Munro for freely distributing his Yorick programming language (available at `ftp://ftp-icf.llnl.gov:/pub/Yorick`) which was used to implement the fitting routines.

Appendix A: fitting of the barycentre

In this appendix, we demonstrate that fitting an unresolved image of several point sources (i.e. the maximum separation between point sources is much less than the size of the PSF) by a single blurred point source yields a position that is the barycentre of the point sources. We also show that the resulting barycentre coordinates are not biased by a limited field of view or some removed bad data points (which is not the case for a simple barycentre).

If the observed object is constituted by N point sources, the measured data at position x_k is:

$$d_k = n_k + \sum_{i=1}^{N} F_i \, P(x_k - \mu_i) \, , \qquad \text{(A1)}$$

[2] IRAF is distributed by the National Optical Astronomy Observatories, which are operated by the Association of Universities for Research in Astronomy, Inc., under cooperative agreement with the National Science Foundation.

where n_k is the noise (residual), $P(x)$ is the assumed point spread function, hereafter PSF, F_i and μ_i are the brightness and position of the $i^{\rm th}$ source. It is worth noting that the PSF can account for the detector response. For our data, since the detector oversamples the telescope plus turbulence PSF (the pixel size was $\sim 1/6^{\rm th}$ of the seeing), we chose a gaussian PSF model that neglects detector effects such as pixelation.

If the size of the object (i.e. the maximum separation $\max_{i,j}||\mu_i - \mu_j||$) is much smaller than that of the PSF, then the object is unresolved and the whole data can be fitted by a model consisting in a single blurred point source:

$$m_k = F\,P(x_k - \mu)\,, \tag{A2}$$

where the total brightness F and mean position μ are the only parameters of the model. These parameters are customarily obtained by a weighted least square fit, that is by minimizing:

$$\chi^2 = \sum_k w_k\,[m_k - d_k]^2$$

where $w_k = 1/{\rm Var}(d_k)$. The parameters F and μ of the model are therefore solution of:

$$\left\{\begin{array}{rcl}\partial_F\chi^2 &=& 0\\ \partial_\mu\chi^2 &=& 0\end{array}\right. \Leftrightarrow \left\{\begin{array}{rcl}\sum_k w_k\,[m_k - d_k]\,P(x_k-\mu) &=& 0\\ \sum_k w_k\,[m_k - d_k]\,F\,\partial_x P(x_k-\mu) &=& 0\end{array}\right.$$

For sake of simplicity, we consider a frame approximatively centered at the object mean position so that all the positions μ_1, $\ldots$, μ_N and μ are negligible with respect to the size of the PSF. We Taylor expand the PSF at each pixel position around $\mu = 0$:

$$P(x_k - \mu) \simeq p_k - \mu\,g_k\,, \qquad\qquad (\mu \ll {\rm FWHM_{PSF}})$$

where $p_k = P(x_k)$ and $g_k = \partial_x P(x_k)$. From that Taylor expansion, the data and model Eqs. (A1-A2) are approximated by:

$$\begin{aligned} m_k &\simeq F\,p_k - F\,\mu\,g_k\,,\\ d_k &\simeq \left(\sum_{i=1}^N F_i\right) p_k - \left(\sum_{i=1}^N F_i\mu_i\right) g_k + n_k\,. \end{aligned}$$

Under these approximations, the parameters to fit are solution of a linear system and read:

$$\begin{aligned} F_{\rm fit} &\simeq \sum_{i=1}^N F_i + \frac{1}{\Delta}\sum_{k,l} w_k w_l g_l (p_k g_l - p_l g_k) n_k\\ F_{\rm fit}\mu_{\rm fit} &\simeq \sum_{i=1}^N F_i\mu_i + \frac{1}{\Delta}\sum_{k,l} w_k w_l p_l (p_k g_l - p_l g_k) n_k \end{aligned}$$

where

$$\Delta = (\textstyle\sum_k w_k p_k^2)(\sum_k w_k g_k^2) - (\sum_k w_k p_k g_k)^2$$

Since the PSF is approximately symmetrical (an even function), its gradient is an odd function and $\sum_k w_k p_k g_k$ is negligible (unless the field of view is strongly shifted with respect to the barycentre of the observed object); then:

$$F_{\rm fit} \simeq \sum_{i=1}^N F_i + \frac{\sum_k w_k p_k n_k}{\sum_k w_k p_k^2}\,, \tag{A3}$$

$$\mu_{\rm fit} \simeq \frac{\sum_{i=1}^N F_i\mu_i}{\sum_{i=1}^N F_i} - \frac{\sum_k w_k g_k n_k}{\sum_{i=1}^N F_i \sum_k w_k g_k^2}\,, \tag{A4}$$

where the expected values of the bias terms (two last right hand side terms in the above expressions) are zero. This demonstrates that, under the considered approximations, the expected value of the fitted position is the true barycentre $\mu = \sum_i F_i\mu_i / \sum_i F_i$ of the object. It is worth noting that $P(x)$ must not be exactly the true PSF: it is sufficient that the mean weigthed residuals $\sum_k w_k g_k n_k$ have a negligible value.

Eq. (A4) shows that the expected value ${\rm E}(\mu_{\rm fit})$ of the fitted position does not depends on the completeness of the data set: ${\rm E}(\mu_{\rm fit}) = \mu$ even if some bad data points are removed or if the field of view is truncated. This is not the case of the simple barycentre of the data:

$$\bar{\mu} = \frac{\sum_k d_k x_k}{\sum_k d_k}$$

which may be severely biased by the background noise and/or the limited field of view.

References

Bacon R., Adam G., Baranne A., et al., A&AS 113, 347
Barth W., Weigelt G., Zinnecker H., 1994, A&A 291, 500
Bailey J., 1998, MNRAS 301, 161
Cabrit S., Ferreira J., Raga A.C., 1999, A&A 343, L61
Clariá J.J., 1974, A&A 37, 229
Ferreira J., 1997, A&A 319, 340
Filippenko A., 1982, PASP 94, 715
Fischer O., Stecklum B., Leinert Ch., 1998, A&A 334, 969
Hartmann L., Kenyon S.J., Hewett R., et al., 1989, ApJ 338, 1001
Herbig G., 1960, ApJS 4, 337
Hessman F.V., Eislöffel J., Mundt R., et al., 1991, ApJ 370, 384
Hirth G.A., Mundt R., Solf J., 1997, A&AS 126, 437
Koresko C.D., Beckwith S.V.W., Ghez A.M., Matthews K., Neugebauer G., 1991, AJ 102, 6, pp. 2073
Lamzin S.A., Teodorani M., Errico L., et al., 1998, Ast. Rep. 42, 630
Lavalley C., Cabrit S., Dougados C., Ferruit P., Bacon R., 1997, A&A 327, 671
Poetzel R., Mundt R., Ray T.P., 1989, A&A 224, L13
Ray T.P., Mundt R., Dyson J.E., Fallem S.A., Raga A.C., 1996, ApJ 468, L103
Rigaut F., Salmon D., Arsenault R., et al., 1998, PASP 110, 152
Snyder D.L., Hammond A.M., White R.L., 1993, J. Opt. Soc. Am. A 10, 1014
Thiébaut E., 1994, Ph.D. Thesis, Université de Paris 7 (France)
Thiébaut E., Bouvier J., Blazit A., et al., 1995, A&A 303, 795
Welty, A., Strom S.E., Edwards S., Kenyon S.J., Hartmann L.W., 1992, ApJ 397, 260
Whitney B.A., Clayton G.C., Shulte-Ladbeck R.E., et al., 1993, ApJ 417, 687 (W93)